Gassenmeier, M., Sens-Schönfelder, C., Eulenfeld, T., Bartsch, M., Victor, P., Tilmann, F., Korn, M. (2016): Field observations of seismic velocity changes caused by shaking-induced damage and healing due to mesoscopic nonlinearity. - *Geophysical Journal International*, *204*, 3, pp. 1490—1502.

DOI: http://doi.org/10.1093/gji/ggv529

Geophysical Journal International

Geophys. J. Int. (2016) **204,** 1490–1502 doi: 10.1093/gji/ggv529
GJI Seismology

Field observations of seismic velocity changes caused by shaking-induced damage and healing due to mesoscopic nonlinearity

M. Gassenmeier,[1,2] C. Sens-Schönfelder,[1] T. Eulenfeld,[3,*] M. Bartsch,[1] P. Victor,[1] F. Tilmann[1,4] and M. Korn[2]

[1]*Helmholtz Centre Potsdam, German Research Centre for Geosciences GFZ, Telegrafenberg, Section* 2.4, *D*-14473 *Potsdam, Germany. E-mail: martina.gassenmeier@gfz-potsdam.de*
[2]*Institute of Geophysics and Geology, University Leipzig, Talstraße* 35, *D*-04103 *Leipzig, Germany*
[3]*Federal Institute for Geosciences and Natural Resources BGR, Stilleweg* 2, *D*-30655 *Hannover, Germany*
[4]*Institute of Geological Science—Geophysics, Freie Universität Berlin, Malteserstr.* 74-100, *D*-12249 *Berlin, Germany*

Accepted 2015 December 9. Received 2015 November 25; in original form 2015 June 3

SUMMARY

To investigate temporal seismic velocity changes due to earthquake related processes and environmental forcing in Northern Chile, we analyse 8 yr of ambient seismic noise recorded by the Integrated Plate Boundary Observatory Chile (IPOC). By autocorrelating the ambient seismic noise field measured on the vertical components, approximations of the Green's functions are retrieved and velocity changes are measured with Coda Wave Interferometry. At station PATCX, we observe seasonal changes in seismic velocity caused by thermal stress as well as transient velocity reductions in the frequency range of 4–6 Hz. Sudden velocity drops occur at the time of mostly earthquake-induced ground shaking and recover over a variable period of time. We present an empirical model that describes the seismic velocity variations based on continuous observations of the local ground acceleration. The model assumes that not only the shaking of large earthquakes causes velocity drops, but any small vibrations continuously induce minor velocity variations that are immediately compensated by healing in the steady state. We show that the shaking effect is accumulated over time and best described by the integrated envelope of the ground acceleration over the discretization interval of the velocity measurements, which is one day. In our model, the amplitude of the velocity reduction as well as the recovery time are proportional to the size of the excitation. This model with two free scaling parameters fits the data of the shaking induced velocity variation in remarkable detail. Additionally, a linear trend is observed that might be related to a recovery process from one or more earthquakes before our measurement period. A clear relationship between ground shaking and induced velocity reductions is not visible at other stations. We attribute the outstanding sensitivity of PATCX to ground shaking and thermal stress to the special geological setting of the station, where the subsurface material consists of relatively loose conglomerate with high pore volume leading to a stronger nonlinearity compared to the other IPOC stations.

Key words: Interferometry; Transient deformation; Site effects; Wave scattering and diffraction; Wave propagation; Fractures and faults.

1 INTRODUCTION

Seismic methods can be used to investigate the internal structure of the Earth and its dynamic changes. This knowledge is crucial to understand the evolution of the Earth in the past, presence and future. The velocity of seismic waves is one observable for the investigation of the Earth's interior. Likewise changes of the seismic velocities can be used to study internal processes. Variations in seismic velocity can be monitored at high precision with repeated artificial sources like vibrator sources or explosions (Li *et al.* 1998; Nishimura *et al.* 2000; Wegler *et al.* 2006). The disadvantage of such investigations can be either high costs for the operation of repeatable sources or a poor temporal sampling. Poupinet *et al.* (1984), Ratdomopurbo & Poupinet (1995), Schaff & Beroza (2004) and

*Former name: T. Richter.

Pandolfi *et al.* (2006) showed that it is also possible to use the coda of earthquake multiplets to extract temporal variations in seismic velocity. This approach is inexpensive but prevents any control over the timing of observations that completely relies on the irregular occurrence of earthquakes. As suggested by Poupinet *et al.* (1984), the key to the precise observation of minute changes is the use of the scattered seismic wavefield that forms the coda of seismic records. This concept was extended and termed Coda Wave Interferometry by Snieder *et al.* (2002) and Snieder (2006). Coda waves are highly sensitive to changes of subsurface properties because they accumulate the effect of medium changes during their extended propagation time. To overcome the dependency on expensive active sources or uncontrolled irregularly occurring earthquakes, Sens-Schönfelder & Wegler (2006) proposed ambient seismic noise as continuously available source and called this approach Passive Image Interferometry (PII).

The main processing step in seismic interferometry is to calculate cross- or autocorrelation functions of the seismic observations that represent approximations of the Green's function between the stations. The cross-correlation can be interpreted as the wavefield that would be measured if a source was placed at one station and a receiver at the other. Reviews and tutorials are given in Curtis *et al.* (2006) and Wapenaar *et al.* (2010). The velocity change can be derived by comparing individual correlation functions derived from seismic measurements recorded at different times. Again it is usually the scattered coda part of the correlation functions which is used to infer medium changes. Besides their high sensitivity to medium changes, coda waves are less influenced by changes in the noise source distribution than direct waves, resulting in reliable estimates of velocity changes (Colombi *et al.* 2014).

A velocity variation can be caused by different processes in the subsurface: at Piton de la Fournaise volcano a drop in seismic velocity was systematically detected before eruptions (Brenguier *et al.* 2008b). Sens-Schönfelder *et al.* (2014) observed an increase of velocity associated with subsidence during post-eruptive periods of deflation. PII was also applied for landslide monitoring (Mainsant *et al.* 2012) showing a decrease in velocity prior to a landslide indicating the creation of weaknesses in the monitored material. On the moon, Sens-Schönfelder & Larose (2010) observed periodic velocity variations that were interpreted as induced by temperature variations. On Earth seasonal changes of seismic velocity have been reported by Sens-Schönfelder & Wegler (2006), Hobiger *et al.* (2012), Meier *et al.* (2010), Richter *et al.* (2014) and Gassenmeier *et al.* (2015). The processes causing these seasonal changes strongly depend on the study area: Sens-Schönfelder & Wegler (2006) modeled the seasonal variations at Merapi volcano with changes in fluid saturation of the medium due to precipitation and groundwater level changes. In Germany, Gassenmeier *et al.* (2015) observed a direct correlation between velocity change and groundwater level data as well as a sharp increase in seismic velocity due to ground frost. In the Los Angeles basin, Meier *et al.* (2010) attributed the velocity variations mainly to thermoelastically induced strain variations in the upper crust. With data from a very dry region in Chile, Richter *et al.* (2014) derived a model for the annual variations based on thermally induced stress described in more detail in Section 3.1.1. Velocity drops after large earthquakes followed by a slow recovery were detected by Rubinstein & Beroza (2004a), Li *et al.* (2007), Brenguier *et al.* (2008a),Wegler *et al.* (2009), Nakata & Snieder (2011), Takagi *et al.* (2012), Hobiger *et al.* (2012), Richter *et al.* (2014) and other authors. In particular, Richter *et al.* (2014) showed that the amplitude of the velocity drop after an earthquake is proportional to the local peak ground acceleration (pga).

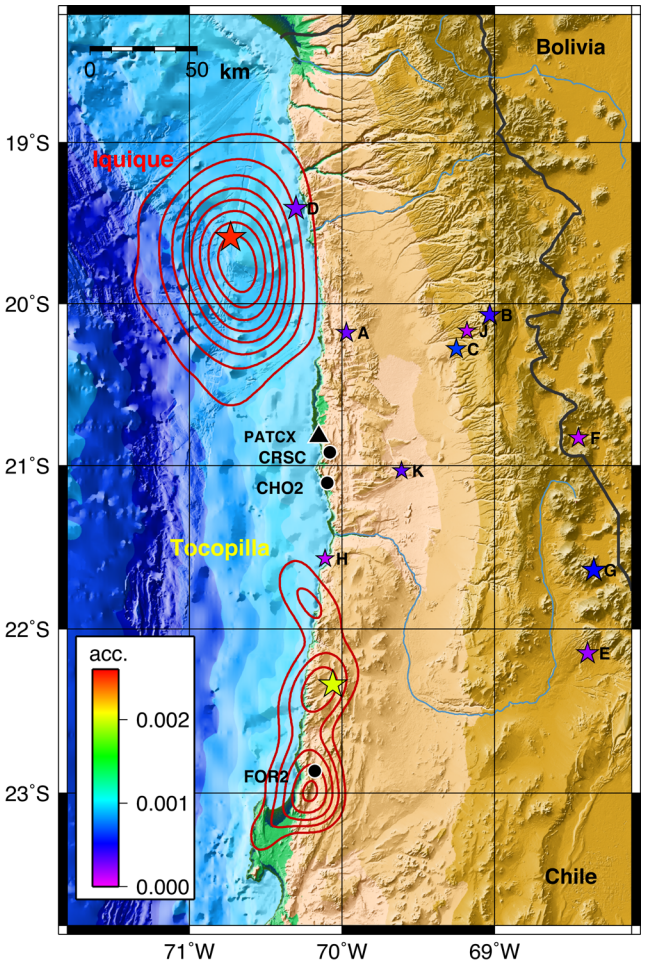

Figure 1. Map of Northern Chile with station PATCX and selected earthquakes corresponding to Table 1. The symbol size corresponds to the magnitude and the colour code represents the acceleration integrated over the day of the earthquake at PATCX in metres per second. For the Tocopilla earthquake on 2007 November 14 and the Iquique earthquake on 2014 April 1 the rupture slip distribution of these earthquakes from Schurr *et al.* (2012, 2014) are displayed with red isolines (0.5–3 m for the Tocopilla event and 0.5–5 m for the Iquique event). The GPS (CRSC) and the creepmeter stations (FOR2, CHO2) shown in Fig. 3 are plotted with black circles.

In this paper, we provide further evidence for the origin of seasonal velocity changes and demonstrate that measureable velocity reductions due to shaking are not only caused by large earthquakes but also by smaller ones. We suggest that even small vibrations continuously induce velocity drops that are normally rapidly compensated.

2 DATA AND METHOD

We work with data recorded by station PATCX from the Integrated Plate Boundary Observatory Chile network (IPOC) of GFZ & CNRS-INSU (2006) in Northern Chile between 18° and 25°S (Fig. 1). Subduction of the Nazca Plate underneath the South American Plate causes intense seismicity in the region. In our study period from 2007 to 2014, two major earthquakes occurred in this area: the M_W 7.7 Tocopilla earthquake on 2007 November 14 and the M_W 8.1 Iquique earthquake on 2014 April 1. Cross-correlating different station pairs in the frequency band of 0.01–0.5 Hz did not show any considerable velocity changes as already indicated by

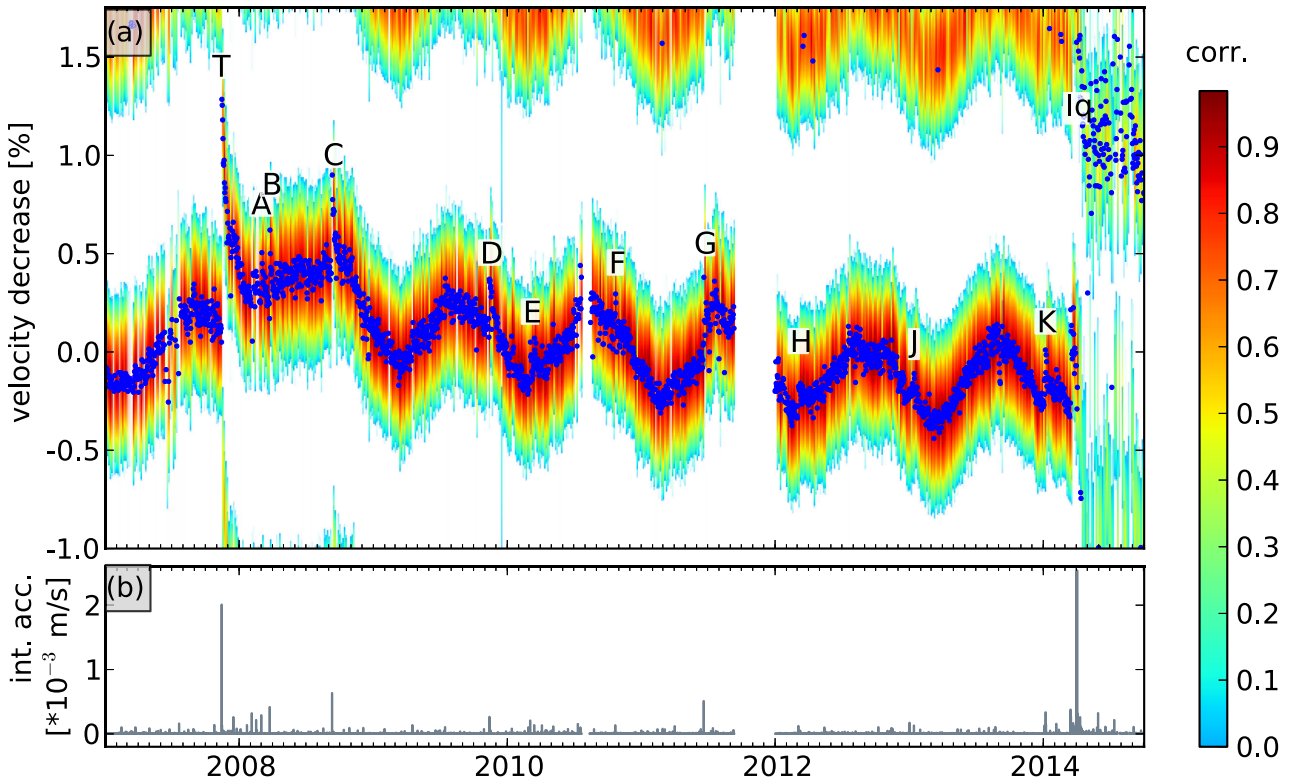

Figure 2. (a) Similarity matrix (R) of station PATCX between 10–15 s and 4–6 Hz. Negative correlation coefficients appear white. The blue dots in the similarity matrix symbolize the daily velocity variations δv. The rare blue dots at velocity decreases larger than 1.5 per cent before 2014 April result from cycle skipping. The M_W 7.7 Tocopilla and the M_W 8.1 Iquique earthquake are marked with T and Iq, respectively. A–K mark selected earthquakes corresponding to Table 1 and Fig. 1. The absolute ground acceleration integrated over one day at station PATCX is plotted with black bars in (b).

Richter *et al.* (2014). We therefore calculate high-frequency daily autocorrelations for the vertical components in the frequency ranges of 1–3 Hz, 4–6 Hz and 7–10 Hz. We follow the processing scheme of Richter *et al.* (2014) with the aim to have a consistent database for analysing velocity changes with PII. In the pre-processing, the waveforms are downsampled to 50 Hz, detrended and filtered. To recover the Green's function as faithfully as possible, we would like to suppress the unwanted effect of earthquakes, which occur very frequently in this seismically active area. Therefore, time windows with an envelope larger than 10 times the root mean square of the envelope in quiet periods are detected and set to zero. We make sure that the deleted time windows are at least two minutes long and we taper the edges in order to avoid artefacts in the autocorrelation function (ACF) at small lapse times. Additionally, 1-bit normalization is applied before calculating daily ACFs.

Relative velocity changes ($\Delta v/v = \delta v$) were measured with the stretching method (Sens-Schönfelder & Wegler 2006; Hadziioannou *et al.* 2009, 2011), which compares individual ACFs ($\phi(t_i, \tau)$) calculated from noise signal that was recorded at time t_i to stretched or compressed versions of a long-term averaged reference ACF $\xi(\tau)$. Here τ indicates the lapse time of the ACF, that is, the traveltime of waves. For each time window and each velocity change $\delta\epsilon_j$, the comparison between ϕ and ξ is performed in terms of the correlation coefficient

$$R(t_i, \epsilon_j) = \int_{\tau_1}^{\tau_2} \phi(t_i, \tau)\xi\left(\tau * (1 + \epsilon_j)\right) d\tau \qquad (1)$$

of a set of stretching values ϵ_j in a lapse time window (τ_1, τ_2). The set of correlation coefficients R for all times t_i and stretching values ϵ_j is hereafter referred to as similarity matrix. The stretching value ϵ_m that results in the maximum correlation $R(t_i, \epsilon_m)$ yields the relative velocity change $\delta v(t_i) = \epsilon_m$ at time t_i. The stretching was implemented in the range of ± 3.3 per cent and the temporal resolution of the velocity change estimation is one day. To gain the highest sensitivity for velocity changes, we use the frequency range of 4–6 Hz and the lag time window between 10 and 15 s (Richter *et al.* 2014). Lower frequencies were found to be less sensitive for shaking-induced velocity variations and higher frequencies led to velocity variations with a lower signal-to-noise ratio (see Supplementary Material Fig. S1). The velocity changes were also estimated in lag time windows between 5–10 and 15–20 s showing identical features, but with a lower signal-to-noise ratio (see Supplementary Material Fig. S2). For the calculation of the reference trace, we use an iterative process (Richter *et al.* 2014) in which a preliminary reference trace is calculated as the mean over all autocorrelation traces, leading to a preliminary estimate of the velocity changes. In a second step, the ACFs are corrected for the preliminary estimated velocity changes and a final reference trace is calculated as the mean over the corrected autocorrelation traces. For high frequencies and late lag times, this two-step approach minimizes the problems of cycle skipping although it cannot eliminate it completely. Such instances are easily identified by consideration of neighboring days (Fig. 2). In order to validate the reliability of the measurement, we repeated the velocity change estimation with autocorrelations for the horizontal components for a time between 2012 and 2014. The results show comparable velocity variations—confirming the results estimated with the vertical component (see Supplementary Material Fig. S1).

Table 1. Selected earthquakes.

	Time	Lat (°)	Lon (°)	Depth (km)	Mag.	Source	Dist. (km)
A	2008 March 1	−20.31	−69.98	40	5.6 (M_W)	EMSC	59
B	2008 March 24	−20.08	−68.97	121	6.2 (M_W)	EMSC	148
C	2008 September 10	−20.28	−69.25	10	5.8 (M_W)	EMSC	112
D	2009 November 13	−19.41	−70.30	43	6.5 (M_W)	EMSC	157
E	2010 March 4	−22.15	−68.39	108	6.3 (M_W)	EMSC	235
F	2010 October 22	−20.83	−68.45	97	5.7 (M_W)	EMSC	177
G	2011 June 20	−21.64	−68.35	128	6.5 (M_W)	EMSC	208
H	2012 March 4	−21.57	−70.11	42.7	5.1 (M_W)	ISC	83
J	2013 January 13	−20.17	−69.18	90	5.4 (m_b)	EMSC	124
K	2014 January 7	−21.03	−69.61	92	5.3 (M_W)	EMSC	61

3 SEISMIC VELOCITY CHANGES

At station PATCX, we observe periodic and transient velocity variations (Fig. 2). Sharp decreases in seismic velocity occur at the time of increased ground shaking. The abrupt decay is followed by a gradual recovery. This behaviour can be observed at the time of the M_W 7.7 Tocopilla event on 2007 November 14 and of the M_W 8.1 Iquique earthquake on 2014 April 1. The absolute velocity effect of the Iquique event is significantly larger than the effect of the Tocopilla event. Additionally numerous smaller transients are visible with sharp decreases of seismic velocity with lower amplitude. These signals can be attributed to the shaking caused by smaller local earthquakes. We selected 10 clearly visible transients denoted with letters A–K in Fig. 2 and investigated the acceleration records of the respective day. For each of the selected days, we could identify one dominating earthquake signal for which we list the source parameters in Table 1. On the other hand, no acceleration peak can be observed in Fig. 2 that is not accompanied by a transient velocity drop. The transient changes are superimposed on a very regular annual cycle over the whole period of investigation. The time after the Iquique earthquake is influenced by a large number of aftershocks and strong medium changes, that lead to a lower correlation value of the stretched correlation function with the reference trace and thus more scatter in the location of the maxima. The velocity at other IPOC stations (see Supplementary Material Figs S5 and S6) are either very stable or the similarity matrices are more noisy than the one for PATCX.

3.1 Physical processes causing the velocity variations

The observed velocity variations can have different physical causes. In the following, we try to distinguish between processes responsible for the annual and transient velocity changes to motivate the modeling that will be introduced in Section 4.1.

3.1.1 Annual velocity changes

Velocity variations with annual periodicity were already observed at PATCX by Richter *et al.* (2014). Additionally, Richter *et al.* (2014) analysed data at a temporal resolution below one day, and identified velocity changes with a period of 24 h. Except for a phase shift, both annual and daily velocity changes, correlate perfectly with air temperature. This leads to the assumption of an atmospheric origin of the velocity changes. Depending on the lapse time window used for their analysis, Richter *et al.* (2014) observe phase delays between velocity changes and surface temperature of a few hours for the daily and approximately 30 d for the annual changes.

Richter *et al.* (2014) presented a model based on thermally induced stress, which explains the observed seismic velocity changes. Increased temperature can lead to stress build-up. In turn, this changes the elastic properties and the velocity of the medium. The subsurface temperature fluctuations were assumed to be spatially periodic, similar to the formulation of Berger (1975). These lateral variations are caused by topography and the presence of the ocean leading to high temperature variations in the mountains and low variations at the shoreline. Solving the heat equation leads to temperature fluctuations exponentially decreasing and experiencing a phase shift with depth. The temperature related stress changes together with experimentally determined values of the elastic properties can be used to predict the velocity changes.

Because of the laterally varying temperature changes the thermal stresses should also induce periodic surface deformations that must be observable in continuous displacement measurements with global positioning system (GPS) or strain measurements. To test the hypothesis of a thermoelastic origin of the seismic velocity changes, we compare the annual velocity variations at PATCX with continuous GPS and strain data from the IPOC observatory. We selected GPS stations with at least two years of data resulting in a total of 23 stations. After detrending the data, we observed periodic variations in GPS with a period of one year at all stations. As an example the station closest to PATCX is shown in the upper panels of Fig. 3. The maximum amplitude of the annual GPS variations amounts to a few millimetres, with north–south displacements showing stronger variations than the east–west components for all stations except one.

Until 2001, such annual signals in GPS data were attributed to atmospheric influences, until Heki (2001) observed arc-normal contraction up to a few millimetres as well as subsidence up to a few centimetres in Japan and related this to surface loads caused by snow. Dong *et al.* (2002) analysed 4.5 yr of global continuous GPS time-series and showed that 40 per cent of the power of the observed annual vertical variations can be attributed to pole tide effects, ocean tide loading, atmospheric loading, nontidal oceanic mass and groundwater loading. With data from California, Prawirodirdjo *et al.* (2006) suggested that thermoelastic strain contributes significantly to the seasonal periodicity in GPS displacements. Tsai (2011) modeled the effects of thermoelastic strain variations on GPS following Ben-Zion & Leary (1986) and concluded that thermoelastic variations may be responsible for an observable fraction of the annual variability of horizontal GPS displacements but it is not likely to explain the entire annual signal.

Annual signals are also observed in strain measured with several creepmeters that are installed in the IPOC to monitor local deformation across individual faults. These data show transient deformation signals that are often superimposed by an annual signal as shown for stations FOR2 and CHO2 in the lower two panels of Fig. 3.

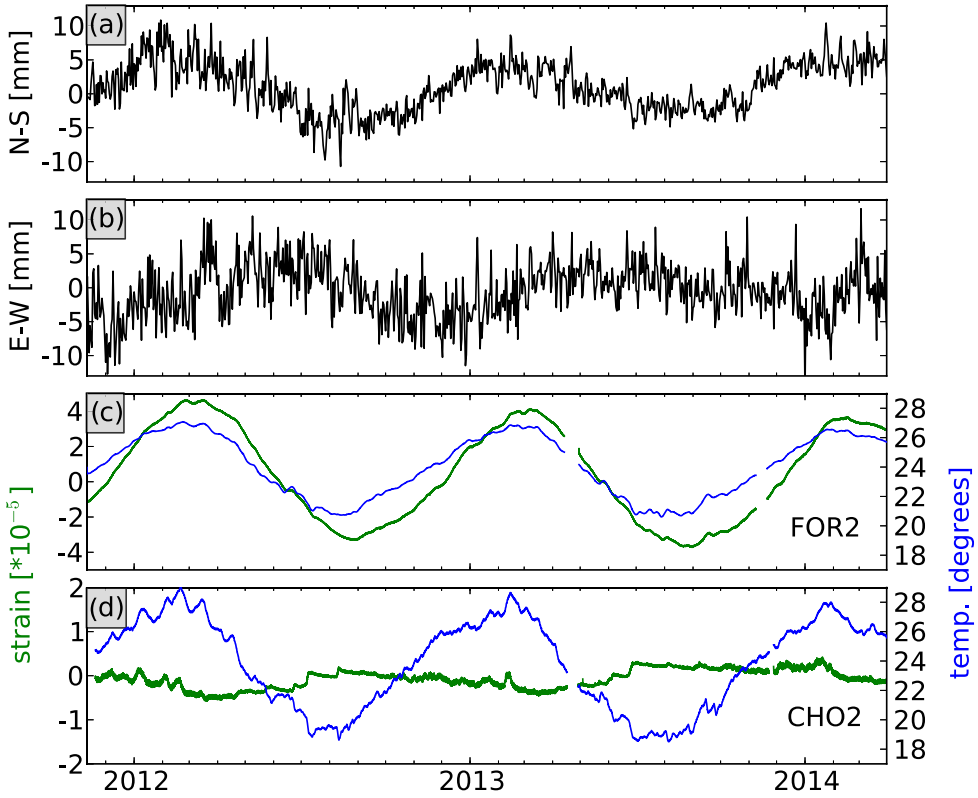

Figure 3. (a) and (b) Annual variations in GPS at station CRSC after removing a linear trend. (c) and (d) Strain variations (green) and temperature (blue) at creepmeter stations FOR2 and CHO2. For the location of these stations we refer to Fig. 1.

For different stations, the strain variations show a highly variable phase shift with respect to temperature. This variability can easily be modeled by an unconsolidated layer that takes part in the heat transport, but does not support stress as it was invoked by Ben-Zion & Leary (1986). This layer might be very different at different sites.

Even though we cannot quantitatively relate the strain and GPS data to the observed velocity variations they provide supporting evidence for the thermoelastic origin of the annual velocity signals. Annual displacement signals as required by the model of Richter *et al.* (2014) are indeed observable. Linear elastic theory cannot explain the variations of the seismic velocities in response to changing ambient stress as it is observed here. The strong annual variations of 0.36 per cent observed at station PATCX indicate a pronounced elastic nonlinearity of the subsurface material.

3.1.2 Transient velocity changes

Sharp coseismic decreases in seismic velocity, followed by a postseismic recovery have been recorded by various authors, as already mentioned in Introduction. The possible physical mechanisms causing this behaviour are discussed in Rubinstein & Beroza (2004a) and Wegler *et al.* (2009). A static coseismic stress change would lead to increases and decreases of stress in different regions depending on the source mechanism. An increase in stress (increased compression) would lead to the closure of pre-existing cracks, involving an increase of velocity, which is rarely—if ever observed. Therefore static stress changes are unlikely to be responsible for the coseismic velocity changes.

With a study of repeated earthquakes and explosions before and after the 2004 Parkfield earthquake, Li *et al.* (2007) observed a decrease in the size of the velocity changes measured in the fault zone with a decrease in slip during the main shock. As mechanism they suggested coseismic damage of fault-zone rocks during the rupture of this earthquake. Analysing repeating earthquakes, Rubinstein & Beroza (2004a,b) observed velocity changes due to the Loma Prieta Earthquake with a very dense network in and around the fault zone. They did not observe any systematic dependence of the velocity changes on the distance to the rupture area.

We calculated 2-D autocorrelation sensitivity kernels according to Pacheco & Snieder (2005) assuming an average S velocity of 1000 ms^{-1} for the near surface and 500 m for the scattering mean-free path. The transport mean-free path characterizes the scattering strength of the medium and is based on studies in volcanic areas (Wegler & Lühr 2001; Yamamoto & Sato 2010) that we think are suitable for the type of material in the shallow subsurface at PATCX. For a traveltime of 12.5 s which is the mean of the time window used for the estimation of the velocity changes we thus estimate that 90 per cent of the sensitivity for the autocorrelation at this lapse time is located in a radius smaller than 2.3 km around the station. As PATCX is about 100 km away from the fault area, we can exclude fault zone damage as responsible mechanism. Furthermore, the nearby GPS station CRSC did not observe any considerable coseismic displacements for the Tocopilla earthquake.

We favour the mechanism of widespread physical damage caused by mesoscopic material nonlinearity in the presence of strong ground motion (Schaff & Beroza 2004). Mesoscopic nonlinearity occurs at microheterogeneities in materials that are composed of constituents with very different elastic properties. Concrete and sandstone or granular materials are prominent examples of such materials where the nonlinearity occurs at weak contacts between competent grains and soft matrix material. In contrast, microscopic or lattice nonlinearity arises due to the nonlinear shape of the

interatomic potential within individual minerals (Nazarov *et al.* 2002). Rubinstein & Beroza (2004a), Peng & Ben-Zion (2006), Rubinstein *et al.* (2007) and Hobiger *et al.* (2012) observed higher velocity changes at sites with larger ground shaking and Richter *et al.* (2014) found a linear relationship between the size of the velocity change and pga at the station investigated here. This leads to the hypothesis that the velocity reductions can be caused by damage. As a nonlinear effect, part of the seismic energy is spent in opening of new or pre-existing cracks or reduced packing of granular material near the surface. This increase in porosity and the reduction of contact area results in a decrease of the elastic moduli of the medium leading to a decrease in the seismic velocities.

With a network of boreholes at 70–350 m depth and surface seismometers, Rubinstein & Beroza (2005) observed that the velocity changes due to the 2004 Parkfield earthquake are located near the surface. This observation supports the theory of nonlinearity causing the velocity changes, because the strength of nonlinearity is inversely related to the effective pressure (Zinszner *et al.* 1997; Ostrovsky *et al.* 2000; Shapiro 2003) and should therefore be concentrated near the surface. Based on records of the Kobe (Pavlenko & Irikura 2003) and Tottori (Pavlenko & Irikura 2006) earthquakes in Japan, nonlinearity of the soil response with changes in rheological properties at depths of 15–25 m were found for stations at distances of 7–80 km from the epicentre, whereas the nonlinearity was stronger for the closer stations. For station PATCX, Richter *et al.* (2014) found the velocity changes measured in the 2–4 Hz band to be weaker by a factor of 1.6 compared to the changes in the 7–9 Hz band, which implies that the velocity changes must be generated in relatively shallow depths, which favours nonlinearity effects also in this study. A precise analysis of the depth where the velocity changes occur would require the correct identification of the wavefield properties. Based on the assumption that the seismic coda is dominated by surface waves (Obermann *et al.* 2013), we can obtain a rough depth estimate of the volume influencing the measurements. As there is no local velocity model available for the surroundings of station PATCX, we use an idealized half-space model with p-wave velocity $v_p = 2000\,\mathrm{ms}^{-1}$, s-wave velocity $v_s = 1000\,\mathrm{ms}^{-1}$ and density $\rho = 2.5\,\mathrm{g\,cm}^{-3}$. For such a velocity structure, 90 per cent of the integrated depth-dependent Rayleigh wave sensitivity is located above a depth of 114 and 168 m for frequencies of 6 and 4 Hz, respectively. At shallow depth, velocities can be expected to be below the values assumed above for the half-space. This would shift the 90 per cent sensitivity limit even to shallower depth.

After the damaging event cracks close and the granular material consolidates again in a post-seismic healing process approaching asymptotically the level prior to the earthquake. In nonlinear dynamics, laboratory experiments with sedimentary and crystalline rocks show a logarithmic recovery process of the resonance frequency or velocity after a strain less than 10^{-6} is applied. This behaviour is called 'slow dynamics'. For an experimental overview of slow dynamic processes in different fields, we refer to TenCate (2011) and references therein. Tremblay *et al.* (2010) used Diffuse Acoustic Wave Spectroscopy to show that slow dynamics occurs, at least in part, due to tiny structural rearrangements at intergrain contacts. A direct observation of the relation between the nonlinear effects generated at the microheterogeneity and the slow dynamic process after a disturbance in a granular material is described by Zaitsev *et al.* (2005). This shows that similar to the stress-induced changes also changes induced by transient shaking occur in the medium at those contacts that are responsible for the nonlinear behaviour of the bulk. Considering a single Hertzian contact (Johnson 1985) between two beads which are subjected to a static and dynamic deformation, Tournat *et al.* (2004) showed that the contact nonlinearity increases with decreasing contact strain. This means that the nonlinearity is generated by the weakest contacts of grains or cracks. Attributing the size of the velocity reductions to the site characteristics, Rubinstein & Beroza (2004a) found that stations in sedimentary settings (marine and nonmarine) observe large velocity changes, and the largest of them are observed at the sites located on the youngest rock. We observe a high sensitivity to ground shaking and (thermal) stress at station PATCX, where the near-surface material consists of a loose conglomerate (R. Armijo, 2015, personal communication; Fig. 4). The environment is influenced by evaporites (salt gypsum) due to the vicinity of Salar Grande, a salt lake located in a depression in the Coastal Region of Tarapacá. Visual inspection of the material (Fig. 4) reveals large pore space with irregular aspect ratios that is partly filled with mineralisations. These mineralisations are formed by material that is dissolved in water provided by regularly occurring fog and recrystallises locally as the amount of water is too small for significant transport. In analogy to concrete such material is called gypcrete due to its cementation with gypsum. We hypothesize that this particular composition leads to a stronger mesoscopic nonlinearity compared to other IPOC sites that is responsible for (1) the high stress sensitivity, (2) the high sensitivity to shaking and (3) the slow dynamics that we observe in the recovery process.

4 MODELLING OF SEISMIC VELOCITY CHANGES

In the following section, we present an empirical model for the annual and transient velocity changes. Peng & Ben-Zion (2006) observed a strong correlation between coseismic delays and intensities of strong ground motion generated by the Düzce main shock. For several earthquakes between 2007 and 2011, Richter *et al.* (2014) found a linear relationship between transient velocity change and pga at station PATCX. In foreshock or aftershock periods of large earthquakes, two or more earthquakes can occur in very short intervals, which leads to the question of how to determine the appropriate time interval in which the pga must be calculated as input to the model. Based on aforementioned laboratory results, we expect that not only the shaking of earthquakes induces velocity drops, but any small vibrations continuously induce minor velocity reductions that are immediately compensated by healing in the steady state. Snieder & Beukel (2004) showed that the compaction of a column of glass beads that was subjected to vertical tapping depends on the accumulated deviatoric strain. To take into account the accumulated effect of every small vibration, we calculate the integrated envelope of the ground acceleration over one day, which is the discretization interval of the autocorrelation measurements. We expect a linear relationship between the velocity change and this integrated acceleration due to the linear relation to pga found by Richter *et al.* (2014).

We observe that the recovery time is correlated with the size of the coseismic velocity change (Fig. 2). Therefore, we scale the post-seismic recovery time with the inverse of the integrated acceleration. The physical motivation for the dependence of the recovery time on the amplitude of the excitation is that stronger excitation involves larger crack scales with recovery processes that have longer timescales. For the recovery process, we use an exponential function instead of a logarithmic function often used in the fitting of laboratory experiments, as it converges to a finite limit at large times representing the state of closed cracks before the damaging event.

Figure 4. Map of the surroundings of station PATCX. The station is located at an altitude of 830 m. The next paved road has a minimal distance of 2.6 km. A power plant is located on the peninsula at a distance of 4.3 km and a copper dehydration plant is located 4.8 km NNW. The blue circle illustrates the region of sensitivity for the autocorrelations (see Section 3.1). The material at the station, a conglomerate, is shown at the right. (Map: Google, map data: NNES/Astrium, Digital Globe; pictures: B. Schurr).

4.1 Description of the model

We model the velocity changes with three different terms and six free parameters $c_1 \ldots c_6$:

$$\delta v_{\text{mod.}} = \delta v_{\text{seasonal}} + \delta v_{\text{shaking}} + \delta v_{\text{linear}} \tag{2a}$$

The first term describes seasonal changes, modeled by a sine function:

$$\delta v_{\text{seasonal}} = c_1 \sin\left(\frac{2\pi}{1\text{yr}}(t - c_2)\right), \tag{2b}$$

the second term expresses daily transient velocity changes due to ground shaking and its recovery

$$\delta v_{\text{shaking}} = c_3 \sum_{i=0}^{N} \left(a(t_i) \exp\left(-\frac{(t - t_i)}{c_4 a(t_i)}\right) H(t - t_i)\right) \tag{2c}$$

and the last term describes a continuous decrease in velocity:

$$\delta v_{\text{linear}} = c_5 + c_6 t. \tag{2d}$$

c_1 and c_2 are the amplitude of the annual velocity changes and the phase relative to January 1. The term $a(t_i)$ is the integrated envelope of the ground acceleration over day i. The amplitude of the transient velocity reductions and the recovery time are proportional to $a(t)$ and c_3 and c_4 are the constants of proportionality. $H(t - t_i)$ is the Heaviside function yielding 1 for $t > t_i$ and 0 otherwise. A long-term linear trend in velocity is described by the y-intercept c_5 and the slope c_6. In the beginning, we did not use the last term in eq. (2a), which resulted in overpredicted velocity decreases at the beginning of the study period and underpredicted decreases at the end. Introducing this additional linear term removes this behaviour completely. The interpretation of this term will be discussed in Section 5.3. The parameters c_1 through c_6 of the model are estimated in an optimization procedure in which we fit the velocity variations predicted by the model to the similarity matrix $R(\delta v_j, t_i)$. The value (F) that is optimized is simply the integral of the similarity matrix along the velocity change δv_{mod} predicted by the model $F = \sum_i R(\delta v_{\text{mod}}, t_i)$. This value assumes its maximum if the model follows the red ridge of the similarity matrix shown Figs 2 and 5.

The optimization algorithm was implemented with a SciPy-function, which uses the Nelder–Mead simplex algorithm.

4.2 Model results

The observed velocity variations at station PATCX (Fig. 5b) show a high sensitivity to ground shaking and a pronounced annual

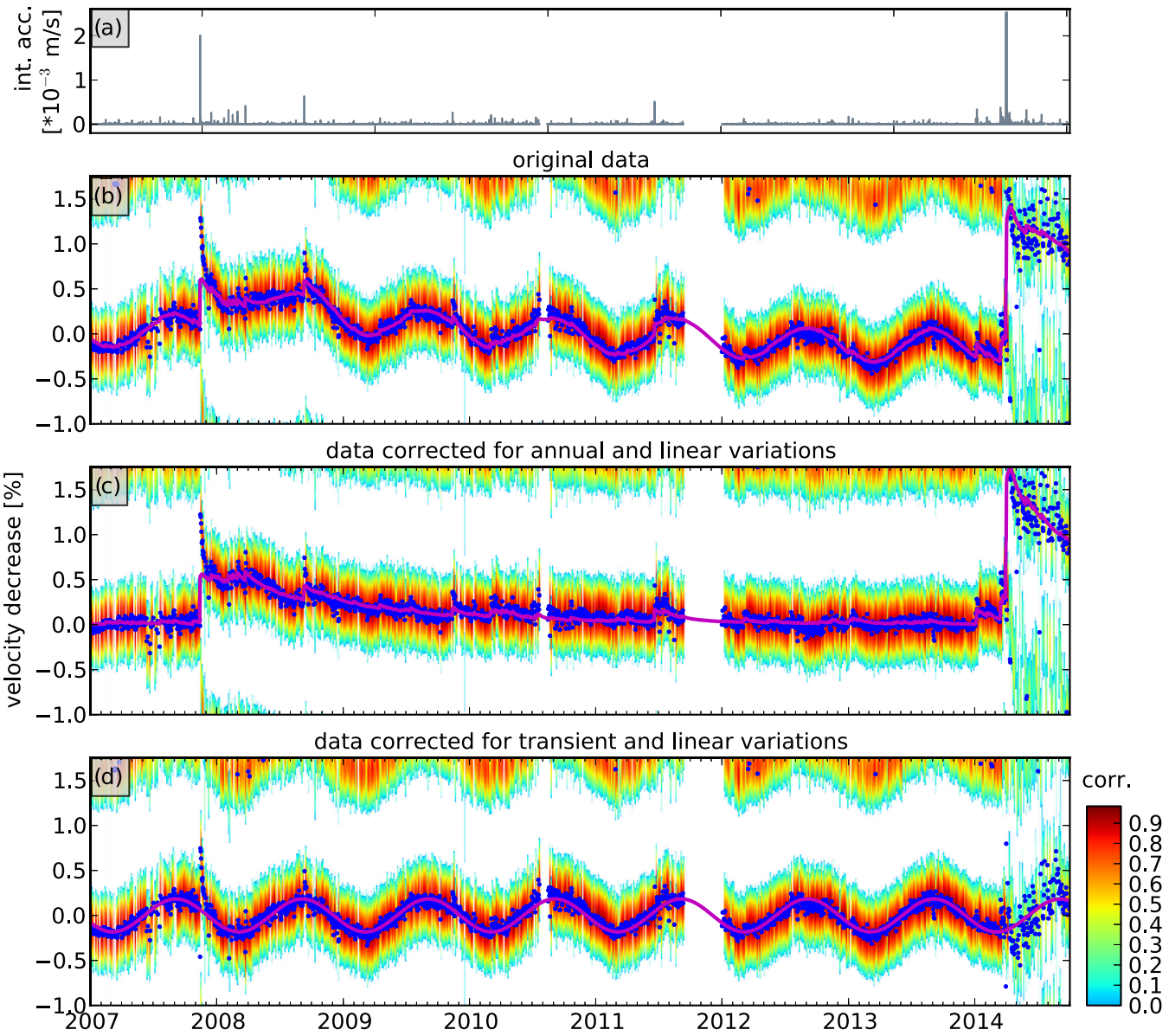

Figure 5. Modeled and observed velocity variations at station PATCX based on 10–15 s lag time in a frequency range of 4–6 Hz: (a) ground acceleration integrated over one day. (b) Complete model function (magenta line) following eq. (2a) superimposed on the similarity matrix. The blue dots symbolize the velocity variations (δv_i) with the largest correlation values. (c) Similarity matrix and the modeled velocity change corrected for the linear and annual variations. (d) Similarity matrix and modeled velocity variations corrected for the linear and transient changes.

variation with a modeled amplitude of 0.18 per cent and a phase delay to the first of January of approximately 155 d, resulting in a maximal velocity decrease at the beginning of September. To emphasize the annual variations, we refer to Fig. 5(d), where we show the annual part of the model (eq. 2b) combined with the observation corrected for the transient and linear term. The transient part of the model combined with the observation corrected for the linear and the seasonal part of the model is shown in Fig. 5(c). Sharp decreases in seismic velocity can be observed at days with an increased acceleration. The long-term decay after the Tocopilla event superimposed by following events with a shorter decay time is clearly visible. For these transient variations, we obtained amplitudes of $2.45 \cdot a(t)$, corresponding to velocity drops of 0.49 and 0.62 per cent for the Tocopilla and the Iquique main shocks, respectively, and the decay times equal to $212020 \cdot a(t)$ d, resulting in 426 d for the Tocopilla event and 535 d for the Iquique event. The decay time represents the time when the velocity has recovered by $1/e$ (37 per cent).

Confidence limits of the model parameters were calculated with the following approach illustrated in Fig. 6: in a first step, we calculate a correlation threshold. Under the assumption that the distribution of the cross-correlation values along the fitted model approximately follows a normal distribution, we calculate the standard deviation of the mean. The threshold of the correlation value is then determined by the maximal correlation value minus one standard deviation. This means that 68 per cent of the fitted values have correlation values above this threshold. To find the confidence limits for one specific parameter, we stepwise change this parameter and run the optimization with the remaining free parameters obtaining lower correlation values between the new model and the similarity matrix. In a last step, we fit a Gaussian distribution to the correlation values obtained with the five free parameters and estimate

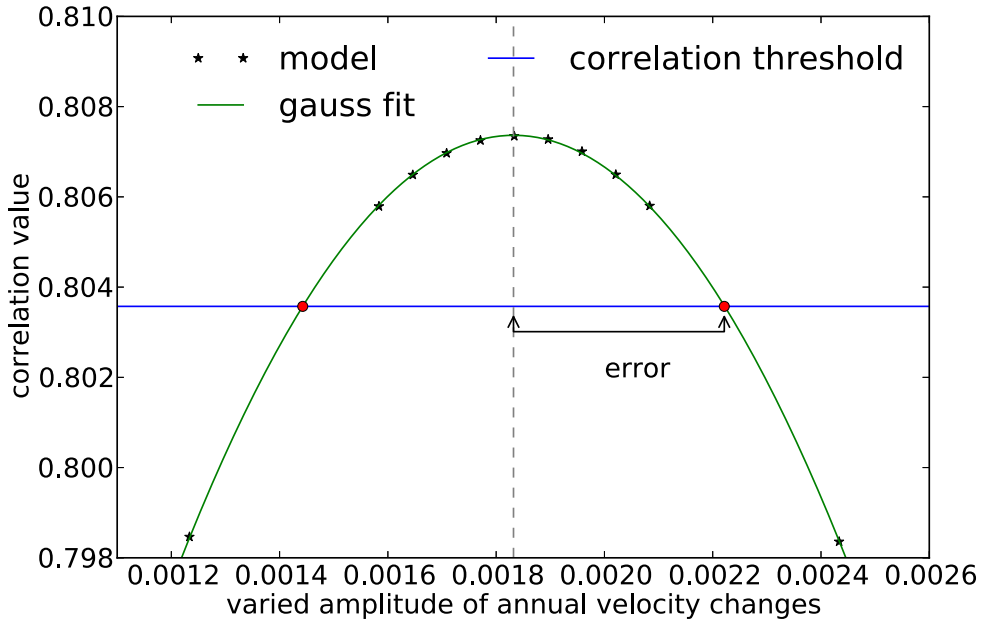

Figure 6. Error estimation of the amplitude of the annual variations (frequency: 4–6 Hz, time window: 10–15 s).

Table 2. Model results c_i and errors Δc_i for PATCX. The velocity change was estimated in a frequency range of 4–6 Hz and a time window of 10–15 s.

i	c_i	Δc_i	Units	
1	0.18	0.039	per cent	Annual changes
2	156	13	days	
3	−2.45	0.45	s m^{-1}	Transient changes
4	212020	71477	days*s m^{-1}	
5	0.022	0.082	per cent	Linear changes
6	0.276	0.108	per cent yr^{-1}	

the intercepts with the threshold correlation value, which gives the error estimate. A visualization of the estimates of the other model parameter can be found in Supplementary Material Fig. S3.

For the amplitude of the annual variations, we obtained a relative error of 21 per cent and for the phase we obtained an error of 13 d. The relative errors for the amplitude of the transient variations is 18 per cent while the error for the decay time equals to 34 per cent. The latter one is quite large, but that was expected as the number of days with small amount of ground shaking highly dominates over the number of days with high amount of ground shaking. For station PATCX, the model parameters and the errors are summarized in Table 2.

The similarity matrices of other stations of the IPOC network are either too noisy or stable (no velocity change), which makes it impossible to fit the model to those observations within reasonable errors (see Supplementary Material Figs S5 and S6). We want to emphasize that the high sensitivity of PATCX to ground shaking described with the presented model can be attributed to the special composition of the near-surface material as described in Section 3.1.2.

5 DISCUSSION

5.1 Seasonal velocity variations

The seasonal changes can be attributed to temperature-induced stress changes. This is supported by the observation of seasonal changes of GPS positions and strain, measured by creepmeters, which show annual variations as required for thermally induced stress. The different strain measurements show a highly variable phase shift with respect to temperature, which could be caused by additional effects due to the complex structure in the vicinity of the faults across which most of the creepmeters are installed. Another possible explanation for the variable phase shifts is the influence of the unconsolidated layer which participates in the heat conduction but does not transfer stress and thereby modulates the phase shift between temperature and strain (Ben-Zion & Leary 1986). The GPS displacement measurements show annual variations as required for the model of thermoelastic stresses by Richter *et al.* (2014). Additional to the E–W displacement that is predicted for an E–W oriented temperature gradient we also observe periodic motion on the N–S components. In fact, the N–S motion has larger amplitude. These displacements might result from the complexity of local structure (Fig. 4) leading to a different gradient direction or might be of different origin. A detailed analysis is beyond the scope of this paper. But we note that strain and displacement data are compatible with a thermoelastic origin of the annual velocity changes.

5.2 Transient velocity variations

Transient velocity decreases after large earthquakes followed by a slow recovery were observed by various authors and widespread physical damage due to ground shaking seems to be the best possible explanation for changes in the shallow subsurface (see Section 3.1.2 for details). Due to the broad distribution of crack sizes in geological media, we do not expect the damage and healing process to occur only if a certain threshold of excitation is exceeded (Beresnev & Wen 1996). Our hypothesis is therefore that not only the ground shaking of large earthquakes induces transient variations in seismic velocity, but every small excitation continuously leads to such transient changes and a recovery afterward. In laboratory experiments, it was shown that the recovery of the elastic moduli follows a linear relation with a logarithmic timescale (Tremblay *et al.* 2010; TenCate 2011). In field measurements, Peng & Ben-Zion

(2006) and Wu *et al.* (2009) observed a logarithmic recovery of a velocity decrease induced by a strong earthquake. These studies always investigate the effect of a single excitation and do not consider the superposition of different relaxation curves. In our case we clearly observe that the healing processes of different events overlap in a way that the effects of smaller events appear superimposed on the long-term effects of larger events. This might indicate an involvement of the medium at different scales. However as the logarithm grows without bounds at large times we cannot use it to model the recovery process of continuous excitations without the definition of a termination condition. Such a departure from the log-time behaviour was observed by TenCate (2011) after 30 min in laboratory experiments. As these observations are obviously not applicable to our field measurements and we are not aware of any experiment investigating how the log-time behaviour changes for very long times, we modeled the recovery process with an exponential law.

Our model for the transient variations has two free parameters and we assume that the amplitude and the recovery time of the exponential function are proportional to the strength of ground shaking. The exponential recovery function in eq. (2c) generally describes the observed velocity changes very well. However, the slope of the decay in the first days after a high acceleration is steeper than the slope modeled with the exponential function, which results in underestimated early amplitudes of the transient variations as illustrated in a scaled stack of the largest transients in Fig. S7. A model with a logarithmic decay including a suitable regularization at zero and infinite timescales might provide a better fit to both the early and late parts of the recovery.

We also fitted the data with a model of constant recovery times independent of the amount of shaking (Fig. S8a). The two models with acceleration-dependent recovery time (model 1) and constant recovery time (model 2) can be compared in the light of the error estimation for the model parameters in Section 4.2. We obtain a mean correlation value of 0.807 (maximum in Fig. 6) for model 1 and 0.797 for model 2. Given the error bound for the mean correlation value (see Fig. 6), model 1 explains the data significantly better than model 2.

Our conclusion that the model with excitation-dependent recovery times is the preferable model is restricted to the limitations of the present data set. Two effects may influence this conclusion. The first effect originates from missing acceleration data before our study period and during recording gaps. As the recovery times of the weak damage from event-free days is very short in model 1, but equal to the one of the largest events in model 2, missing data points influence both models differently. To test the influence of the periods without acceleration data we filled gaps in the acceleration time-series and a five years period prior to our data set with fictitious data (mean of 60 quiet days) and reinverted the data in a separate analysis (Fig. S8b). Resulting parameters for model 1 are very stable whereas the parameters for model 2 change significantly leading to a mean correlation value of 0.805 that is close to model 1.

The second effect that influences the conclusion about the dependency of the recovery time on the excitations originates from the lack of information about significant acceleration events caused by ground shaking of earthquakes prior to our study period. As will be shown in the next section, the linear trend that we observe in the data can be related to the long-lasting recovery of a large event years before our study period if model 1 is used. A model with constant recovery time (model 2) would not be able to explain this observation. Future investigations that will be able to analyse the long-term decay of the large transient caused by the Iquique event will be able to draw more definite conclusions about the amplitude dependence of the recovery time.

5.3 Linear trend

The third contribution in the model is the linear term that describes a slow increase in seismic velocity. This term could reflect the slow healing process of one or several large earthquakes before our study period. As the model is able to estimate a transient velocity change for a given integrated acceleration, it is also possible to calculate the acceleration required for a given velocity change at a given time after the event. We can thus try to investigate whether the linear trend is likely to be caused by an earlier earthquake. Differentiating the model for the transient velocity changes (eq. 2c) with respect to time and equating it with the slope c_6 in the linear term (eq. 2d) leads to a linear dependence between the integrated acceleration and time elapsed since the causative earthquake. The largest earthquake in the vicinity since 1900 was the M_W 9.5 Chile earthquake on 1960 May 22, approximately 2000 km south of PATCX. Given the long time since this event the model predicts a peak velocity change at the time of the earthquake of approximately 10 per cent. This is not realistic for an event at this distance. The two largest earthquakes close to our study area are the M_W 8.4 Arequipa earthquake on 2001 June 23 (∼600 km northwest of PATCX) and the M_W 8.1 Antofagasta earthquake on 1995 July 30 (∼300 km south of PATCX). Assuming that one of these earthquakes caused the linear velocity change our model predicts a velocity change at the time of the earthquakes of approximately 1.2 per cent for the Arequipa earthquake and approximately 2.5 per cent for the Antofagasta earthquake. The Arequipa earthquake led to an intensity of IV–V Modified Mercalli (MM) scale (Tavera *et al.* 2002; USGS shakemap: http://earthquake.usgs.gov/earthquakes/shakemap/atlas/shake/200106232033/, last accessed 28 December 2015), at the region of PATCX, which is lower compared to the intensity of V–VI (USGS shakemap: http://earthquake.usgs.gov/earthquakes/shakemap/atlas/shake/200711141540/, last accessed 28 December 2015) of the Tocopilla earthquake. As the duration of the rupture was 85 s (Tavera *et al.* 2006) which is nearly twice as long as the rupture duration of the Tocopilla earthquake (Delouis *et al.* 2009) we expect a higher integrated acceleration than for the Tocopilla earthquake. The M_W 8.4 Arequipa earthquake in 2001 could therefore have introduced a velocity change of 1.2 per cent leading to the linear trend in the velocity changes that we observe during the study period. As the rupture duration of the Antofagasta earthquake was shorter (60 s; Ruegg *et al.* 1996) compared to the one of the Arequipa earthquake but with a similar maximal shaking (estimated by extrapolation), we conclude that the 1995 earthquake seems less plausible to induce a velocity change of 2.5 per cent which would be necessary to cause the linear trend. Considering that the effects of the different earthquakes are superimposed it seems very likely that the linear trend, which was empirically introduced to fit the data, also consistently results from our model. This indicates that the parameters of the linear trend are related to the initial condition of our model and would not be needed if a sufficiently long history of the acceleration values prior to our study existed.

6 CONCLUSIONS

The outstanding sensitivity of station PATCX to shaking and stress-induced by changes of temperature are interpreted as resulting from

the special composition of the near-surface material, consisting of a soft conglomerate cemented with evaporites (R. Armijo, 2015, personal communication) of around 2.59 Ma age (Sánchez & Cortés 2009).

Both effects reflect elastic nonlinearity in the stress–strain relation. The stress-dependent velocity changes can be related to nonlinearity that arises in granular or microheterogeneous media at Hertzian grain contacts or cracks. In contrast to classical nonlinearity that occurs also in homogeneous media at the atomic scale, the mesoscopic nonlinearity occurs on a larger length scale but below the typical wavelength. In such a medium an increase of the ambient stress closes cracks or increases the intergrain contact area and thereby increases the elastic moduli. This process is the more efficient the weaker the contacts are, that is, it is reduced with the increasing confining pressure at larger depth.

The transient nature of the velocity changes after shaking cannot be explained with this mechanism and requires an additional process. Seismological observations of coseismic velocity changes and the recovery thereafter have been discussed in connection with co- and post-seismic stress changes or hydrological perturbations. We can exclude these causes here based on the convincing match between observed velocity changes and predictions from shaking. Several other mechanisms have been suggested in acoustics that are able to reproduce the characteristic decay that is approximately logarithmic in time. Most of them act on the mesoscopic scale of individual cracks or grain contacts. With experiments on a single crack, Zaitsev *et al.* (2003) demonstrate that the 2-D heat transfer from the 1-D rim of a crack can result in a change of elastic properties that is logarithmic in time. Another process suggested by Zaitsev *et al.* (2014) uses thermal fluctuations of bistable bonds at weak grain contacts to create log-time behaviour. In an ensemble of cracks of different width the model can reproduce even the aging of a granular material that reacts differently on a given excitation depending on previous excitations. These processes critically depend on the presence of weak contacts that are prominent in granular or loosely compacted materials. In fact, the high sensitivity to strain—either dynamic (shaking) or static (temperature induced)—was found to be closely connected to slow dynamics in lab experiments with microheterogeneous geomaterials (Johnson & Sutin 2005).

In analogy to these models that result from acoustic lab experiments, we conclude that also our observations are tightly linked to the physics of the weak contacts in the subsurface material at PATCX. The fact that the material around PATCX is relatively young supports this hypothesis.

However, the processes that lead to the observed changes are not exceptional and occur in almost every material with microheterogeneity. Obviously the parameters that describe these effects will be different. In our empirical parametrization PATCX has exceptionally high values for c_1, c_3 and c_4 indicating a high sensitivity to stress and shaking as well as a slow recovery. We speculate that these parameters empirically describe a more fundamental property of the medium linked to the microheterogeneity, for example, reflected by the crack size distribution, internal surface area or cohesion. We expect that a more detailed analysis of the near-surface material at PATCX and other stations together with microscopic modeling of the observed processes might lead to a new understanding of time-dependent rheology.

ACKNOWLEDGEMENTS

We want to acknowledge the IPOC group for providing the data. We thank Roel Snieder and Marcos Moreno for helpful discussions as well as Thomas Ziegenhagen for providing the creep data. We also thank Günter Asch for maintaining the seismic stations. Comments by the editor Y. Ben-Zion and reviewers M. Hobiger and G. Hillers helped to improve the manuscript.

REFERENCES

Ben-Zion, Y. & Leary, P., 1986. Thermoelastic strain in a half-space covered by unconsolidated material, *Bull. seism. Soc. Am.,* **76**(5), 1447–1460.

Beresnev, I.A. & Wen, K.-L., 1996. Nonlinear soil response—a reality?, *Bull. seism. Soc. Am.,* **86**(6), 1964–1978.

Berger, J., 1975. A note on thermoelastic strains and tilts, *J. geophys. Res.,* **80**(2), 274–277.

Brenguier, F., Campillo, M., Hadziioannou, C., Shapiro, N.M., Nadeau, R.M. & Larose, E., 2008a. Postseismic relaxation along the San Andreas fault at Parkfield from continuous seismological observations, *Science,* **321**(5895), 1478–1481.

Brenguier, F., Shapiro, N.M., Campillo, M., Ferrazzini, V., Duputel, Z., Coutant, O. & Nercessian, A., 2008b. Towards forecasting volcanic eruptions using seismic noise, *Nat. Geosci.,* **1**(2), 126–130.

Colombi, A., Chaput, J., Brenguier, F., Hillers, G., Roux, P. & Campillo, M., 2014. On the temporal stability of the coda of ambient noise correlations, *C. R. Geosci.,* **346**(11–12), 307–316.

Curtis, A., Gerstoft, P., Sato, H., Snieder, R. & Wapenaar, K., 2006. Seismic interferometry turning noise into signal, *Leading Edge,* **25**(9), 1082–1092.

Delouis, B., Pardo, M., Legrand, D. & Monfret, T., 2009. The Mw 7.7 Tocopilla earthquake of 14 November 2007 at the southern edge of the Northern Chile seismic gap: rupture in the deep part of the coupled plate interface, *Bull. seism. Soc. Am.,* **99**(1), 87–94.

Dong, D., Fang, P., Bock, Y., Cheng, M.K. & Miyazaki, S., 2002. Anatomy of apparent seasonal variations from gps-derived site position time series, *J. geophys. Res.,* **107**(B4), ETG 9–1–ETG 9–16.

Gassenmeier, M., Sens-Schönfelder, C., Delatre, M. & Korn, M., 2015. Monitoring of environmental influences on seismic velocity at the geological storage site for CO_2 in Ketzin (Germany) with ambient seismic noise, *Geophys. J. Int.,* **200**(1), 524–533.

GFZ & CNRS-INSU, 2006. IPOC Seismic Network, GFZ German Research Centre for Geosciences, Institut des Sciences de l'Univers-Centre National de la Recherche CNRS-INSU, doi:10.14470/PK615318.

Hadziioannou, C., Larose, E., Coutant, O., Roux, P. & Campillo, M., 2009. Stability of monitoring weak changes in multiply scattering media with ambient noise correlation: laboratory experiments, *J. acoust. Soc. Am.,* **125,** 3688–3695.

Hadziioannou, C., Larose, E., Baig, A., Roux, P. & Campillo, M., 2011. Improving temporal resolution in ambient noise monitoring of seismic wave speed, *J. geophys. Res.,* **116**(B7), B07304, doi:10.1029/2011JB008200.

Heki, K., 2001. Seasonal modulation of interseismic strain buildup in Northeastern Japan driven by snow loads, *Science,* **293**(5527), 89–92.

Hobiger, M., Wegler, U., Shiomi, K. & Nakahara, H., 2012. Coseismic and postseismic elastic wave velocity variations caused by the 2008 Iwate-Miyagi Nairiku earthquake, Japan, *J. geophys. Res.,* **117**(B9), 1–19.

Johnson, K.L., 1985. *Contact Mechanics*, Cambridge Univ. Press.

Johnson, P. & Sutin, A., 2005. Slow dynamics and anomalous nonlinear fast dynamics in diverse solids, *J. acoust. Soc. Am.,* **117**(1), 124–130.

Li, Y.-G., Vidale, J.E., Aki, K., Xu, F. & Burdette, T., 1998. Evidence of shallow fault zone strengthening after the 1992 M7.5 Landers, California, Earthquake, *Science,* **279**(5348), 217–219.

Li, Y.-G., Chen, P., Cochran, E. & Vidale, J., 2007. Seismic velocity variations on the San Andreas fault caused by the 2004 M6 Parkfield Earthquake and their implications, *Earth Planets Space,* **59**(1), 21–31.

Mainsant, G., Larose, E., Brönnimann, C., Jongmans, D., Michoud, C. & Jaboyedoff, M., 2012. Ambient seismic noise monitoring of a clay landslide: toward failure prediction, *J. geophys. Res.,* **117**(F1), F01030, doi:10.1029/2011JF002159.

Meier, U., Shapiro, N.M. & Brenguier, F., 2010. Detecting seasonal variations in seismic velocities within Los Angeles basin from correlations of ambient seismic noise, *Geophys. J. Int.,* **181**(2), 985–996.

Nakata, N. & Snieder, R., 2011. Near-surface weakening in Japan after the 2011 Tohoku-Oki earthquake, *Geophys. Res. Lett.,* **38**(17), L17302, doi:10.1029/2011GL048800.

Nazarov, V.E., Zaitsev, V.Y. & Institute, I.Y., 2002. Nonlinear transformation of acoustic waves in microinhomogeneous media with relaxation, *Acta Acust. United Acust.,* **88,** 40–49.

Nishimura, T., Uchida, N., Sato, H., Ohtake, M., Tanaka, S. & Hamaguchi, H., 2000. Temporal changes of the crustal structure associated with the M6.1 earthquake on September 3, 1998, and the volcanic activity of Mount Iwate, Japan, *Geophys. Res. Lett.,* **27**(2), 269–272.

Obermann, A., Planes, T., Larose, E., Sens-Schönfelder, C. & Campillo, M., 2013. Depth sensitivity of seismic coda waves to velocity perturbations in an elastic heterogeneous medium, *Geophys. J. Int.,* **194**(1), 372–382.

Ostrovsky, L.A., Johnson, P.A. & Shankland, T.J., 2000. The mecha- nism of strong nonlinear elasticity in earth solids, in *Nonlinear Acoustics at the Turn of the Millenium: ISNA 15*, pp. 75–84, eds Lauterborn, W. & Kurz, T., American Institute of Physics, College Park, Maryland.

Pacheco, C. & Snieder, R., 2005. Time-lapse travel time change of multiply scattered acoustic waves, *J. acoust. Soc. Am.,* **118**(3), 1300–1310.

Pandolfi, D., Bean, C.J. & Saccorotti, G., 2006. Coda wave interferometric detection of seismic velocity changes associated with the 1999 M = 3.6 event at Mt. Vesuvius, *Geophys. Res. Lett.,* **33**(6), L06306, doi:10.1029/2005GL025355.

Pavlenko, O.V. & Irikura, K., 2003. Estimation of nonlinear time-dependent soil behavior in strong ground motion based on vertical array data, *Pure appl. Geophys.,* **160**(12), 2365–2379.

Pavlenko, O.V. & Irikura, K., 2006. Nonlinear behavior of soils revealed from the records of the 2000 Tottori, Japan, earthquake at stations of the digital strong-motion network kik-net, *Bull. seism. Soc. Am.,* **96**(6), 2131–2145.

Peng, Z. & Ben-Zion, Y., 2006. Temporal changes of shallow seismic velocity around the karadere-duzce branch of the north anatolian fault and strong ground motion, *Pure appl. Geophys.,* **163,** 567–600.

Poupinet, G., Ellsworth, W. & Frechet, J., 1984. Monitoring velocity variations in the crust using earthquake doublets: an application to the Calaveras Fault, California, *J. geophys. Res.,* **89**(4), 5719–5731.

Prawirodirdjo, L., Ben-Zion, Y. & Bock, Y., 2006. Observation and modeling of thermoelastic strain in Southern California Integrated GPS Network daily position time series, *J. geophys. Res.,* **111**(B2), B02408, doi:10.1029/2005JB003716.

Ratdomopurbo, A. & Poupinet, G., 1995. Monitoring a temporal change of seismic velocity in a volcano: application to the 1992 eruption of Mt. Merapi (Indonesia), *Geophys. Res. Lett.,* **22**(7), 775–778.

Richter, T., Sens-Schönfelder, C., Kind, R. & Asch, G., 2014. Comprehensive observation and modeling of earthquake and temperature-related seismic velocity changes in northern Chile with passive image interferometry, *J. geophys. Res.,* **119**(6), 4747–4765.

Rubinstein, J.L. & Beroza, G.C., 2004a. Evidence for widespread nonlinear strong ground motion in the MW 6.9 Loma Prieta Earthquake, *Bull. seism. Soc. Am.,* **94**(5), 1595–1608.

Rubinstein, J.L. & Beroza, G.C., 2004b. Nonlinear strong ground motion in the M_L 5.4 Chittenden earthquake: evidence that preexisting damage increases susceptibility to further damage, *Geophys. Res. Lett.,* **31**(23), L23614, doi:10.1029/2004GL021357.

Rubinstein, J.L. & Beroza, G.C., 2005. Depth constraints on nonlinear strong ground motion from the 2004 Parkfield earthquake, *Geophys. Res. Lett.,* **32**(14), L14313, doi:10.1029/2005GL023189.

Rubinstein, J.L., Uchida, N. & Beroza, G.C., 2007. Seismic velocity reductions caused by the 2003 Tokachi-Oki earthquake, *J. geophys. Res.,* **112**(B5), B05315, doi:10.1029/2006JB004440.

Ruegg, J.C. *et al.*, 1996. The MW=8.1 Antofagasta (North Chile) earthquake of July 30, 1995: first results from teleseismic and geodetic data, *Geophys. Res. Lett.,* **23**(9), 917–920.

Sánchez, M.C. & Cortés, H.O., 2009. Geological Map: Proyecto relizado con fondos de la Comisión Nacicional del Medio Ambiente (CONAMA) de la Región de Tarapacá, a través de su programa Fondo de Protección Ambiental (FPA), http://www7.uc.cl/geografia/cda/.

Schaff, D.P. & Beroza, G.C., 2004. Coseismic and postseismic velocity changes measured by repeating earthquakes, *J. geophys. Res.,* **109**(B10), B10302, doi:10.1029/2004JB003011.

Schurr, B., Asch, G., Rosenau, M., Wang, R., Oncken, O., Barrientos, S., Salazar, P. & Vilotte, J.-P., 2012. The 2007 M7.7 Tocopilla northern Chile earthquake sequence: implications for along-strike and downdip rupture segmentation and megathrust frictional behavior, *J. geophys. Res.,* **117**(B5), B05305, doi:10.1029/2011JB009030.

Schurr, B. *et al.*, 2014. Gradual unlocking of plate boundary controlled initiation of the 2014 Iquique earthquake, *Nature,* **512**(7514), 299–302.

Sens-Schönfelder, C. & Larose, E., 2010. Lunar noise correlation, imaging and monitoring, *Earthq. Sci.,* **23**(5), 519–530.

Sens-Schönfelder, C. & Wegler, U., 2006. Passive image interferometry and seasonal variations of seismic velocities at Merapi Volcano, Indonesia, *Geophys. Res. Lett.,* **33**(21), L21302, doi:10.1029/2006GL027797.

Sens-Schönfelder, C., Pomponi, E. & Peltier, A., 2014. Dynamics of piton de la fournaise volcano observed by passive image interferometry with multiple references, *J. Volc. Geotherm. Res.,* **276,** 32–45.

Shapiro, S.A., 2003. Elastic piezosensitivity of porous and fractured rocks, *Geophysics,* **68**(2), 482–486.

Snieder, R., 2006. The theory of coda wave interferometry, *Pure appl. Geophys.,* **163**(2–3), 455–473.

Snieder, R. & Beukel, A. v.d., 2004. The liquefaction cycle and the role of drainage in liquefaction, *Granul. Matter,* **6**(1), 1–9.

Snieder, R., Grêt, A., Douma, H. & Scales, J., 2002. Coda wave interferometry for estimating nonlinear behaviour in seismic velocity, *Science,* **295**(3), 2253–2255.

Takagi, R., Okada, T., Nakahara, H., Umino, N. & Hasegawa, A., 2012. Coseismic velocity change in and around the focal region of the 2008 Iwate-Miyagi Nairiku earthquake, *J. geophys. Res.,* **117,** B06315, doi:10.1029/2012JB009252.

Tavera, H., Buforn, E., Bernal, I., Antayhua, Y. & Vilacapoma, L., 2002. The Arequipa (Peru) earthquake of June 23, 2001, *J. Seismol.,* **6**(2), 279–283.

Tavera, H. *et al.*, 2006. The Southern region of Peru earthquake of June 23rd, 2001, *J. Seismol.,* **10**(2), 171–195.

TenCate, J., 2011. Slow dynamics of earth materials: an experimental overview, *Pure appl. Geophys.,* **168**(12), 2211–2219.

Tournat, V., Zaitsev, V., Gusev, V., Nazarov, V., Béquin, P. & Castagnède, B., 2004. Probing weak forces in granular media through nonlinear dynamic dilatancy: clapping contacts and polarization anisotropy, *Phys. Rev. Lett.,* **92,** 085502–085504.

Tremblay, N., Larose, E. & Rossetto, V., 2010. Probing slow dynamics of consolidated granular multicomposite materials by diffuse acoustic wave spectroscopy, *J. acoust. Soc. Am.,* **127**(3), 1239–1243.

Tsai, V.C., 2011. A model for seasonal changes in GPS positions and seismic wave speeds due to thermoelastic and hydrologic variations, *J. geophys. Res.,* **116**(B4), B04404, doi:10.1029/2010JB008156.

Wapenaar, K., Slob, E., Snieder, R. & Curtis, A., 2010. Tutorial on seismic interferometry: Part 2—underlying theory and new advances, *Geophysics,* **75**(5), 75A211–75A227.

Wegler, U. & Lühr, B.-G., 2001. Scattering behaviour at Merapi volcano (Java) revealed from an active seismic experiment, *Geophys. J. Int.,* **145**(3), 579–592.

Wegler, U., Lühr, B.-G., Snieder, R. & Ratdomopurbo, A., 2006. Increase of shear wave velocity before the 1998 eruption of Merapi volcano (Indonesia), *Geophys. Res. Lett.,* **33**(9), L09303, doi:10.1029/2006GL025928.

Wegler, U., Nakahara, H., Sens-Schönfelder, C., Korn, M. & Shiomi, K., 2009. Sudden drop of seismic velocity after the 2004 Mw 6.6 mid-Niigata earthquake, Japan, observed with passive image interferometry, *J. geophys. Res.,* **114**(B6), B06305, doi:10.1029/2008JB005869.

Wu, C., Peng, Z. & Ben-Zion, Y., 2009. Non-linearity and temporal changes of fault zone site response associated with strong ground motion, *Geophys. J. Int.,* **176**(1), 265–278.

Yamamoto, M. & Sato, H., 2010. Multiple scattering and mode conversion revealed by an active seismic experiment at Asama volcano, Japan, *J. geophys. Res.,* **115**(B7), B07304, doi:10.1029/2009JB007109.

Zaitsev, V., Gusev, V. & Castagnede, B., 2003. Thermoelastic mechanism for logarithmic slow dynamics and memory in elastic wave interactions with individual cracks, *Phys. Rev. Lett.,* **90,** doi:10.1103/PhysRevLett.90.075501.

Zaitsev, V.Y., Nazarov, V.E., Tournat, V., Gusev, V.E. & Castagnède, B., 2005. Luxemburg-gorky effect in a granular medium: probing perturbations of the material state via cross-modulation of elastic waves, *Europhys. Lett.,* **70**(5), 607–613.

Zaitsev, V.Y., Gusev, V.E., Tournat, V. & Richard, P., 2014. Slow relaxation and aging phenomena at the nanoscale in granular materials, *Phys. Rev. Lett.,* **112**(10), doi:10.1103/PhysRevLett.112.108302.

Zinszner, B., Johnson, B. & Rasolofosaon, P.N.J., 1997. Influence of change in physical state on elastic nonlinear response in rock: significance of effective pressure and water saturation, *J. geophys. Res.,* **102**(B4), 8105–8120.

SUPPORTING INFORMATION

Additional Supporting Information may be found in the online version of this paper:

Figure S1. Similarity matrices of the PATCX autocorrelations (10–15 s) for different components and different frequencies. Negative correlation coefficients appear white. The blue dots in the similarity matrix symbolize the velocity variations with the best correlation between the stretched ACFs and the reference trace. The absolute ground accelerations integrated over 1 day are plotted with grey bars.

Figure S2. Similarity matrices of the PATCX vertical component autocorrelations (4–6 Hz) for different time windows of 5–10 s, 10–15 s and 15–20 s. Negative correlation coefficients appear white. The blue dots in the similarity matrix symbolize the velocity variations with the best correlation between the stretched ACFs and the reference trace.

Figure S3. Error estimation of every model parameter in the model (frequency: 4–6 Hz, time window: 10–15 s). The integrated correlation values predicted by the model are plotted with black stars and the corresponding Gauss fit is plotted with a green line. The correlation threshold is marked with a blue line.

Figure S4. Map of northern Chile with the IPOC stations used in this study. The color code represents the acceleration integrated over one day at the stations in [m/s]. The outer triangle refers to the accelerations on 01.04.14 (Iquique earthquake) and the inner triangle to the accelerations on 14.11.2007 (Tocopilla earthquake). The rupture slip distribution of these earthquakes from Schurr *et al.* (2012, 2014) are displayed with red isolines (0.5 to 3 m for the Tocopilla event and 0.5 to 5 m for the Iquique event). The gps (CRSC) and the creepmeter stations (FOR2, CHO2) are plotted with black circles.

Figure S5. The upper subplots of each station show the similarity matrices of the IPOC stations shown in Fig. S4 between 10–15 s and 4–6 Hz. Negative correlation coefficients appear white. The blue dots in the similarity matrix symbolize the velocity variations with the best correlation between the stretched ACFs and the reference trace. The absolute ground accelerations integrated over 1 day are plotted with grey bars. The lower subplots for each station show the spectra after event removal as well as the mean amplitude for each day.

Figure S6. Same as in Fig. S5 for the remaining stations.

Figure S7. Isolated responses of several earthquakes between 10–15 s and 4–6 Hz. The letters in the legend refer to events in table 1. The time is scaled by $c_4 \cdot a$, calculated from the integrated acceleration a of each event and the recovery time proportionality factor c_4. The velocity changes are scaled by event with a and the coseismic velocity change amplitude factor, c_3. Thus, the individual fits (model 1) appear similar and the expected curve is illustrated with the magenta line, a simple exponential function.

Figure S8. Comparison of two different models for PATCX between 10–15 s and 4–6 Hz. (a) Model 1 represents the model with the acceleration dependent recovery time (mean correlation coefficient: 0.807). In model 2 the recovery time is independent of the integrated acceleration (mean correlation coefficient: 0.797). (b) As model 1 and model 2 are influenced differently by time gaps and the time before 2007, a fictitious acceleration was estimated as the mean over a quit time period of 60 days. The missing acceleration values of every time gap as well as 5 years before 2007 were filled with this mean acceleration and the minimization was recalculated. The results of model 1^* were similar to model 1 (mean correlation coefficient: 0.807). Model 2^* achieved a mean correlation coefficient of 0.805. Negative correlation coefficients in the similarity matrix appear white. The blue dots in the similarity matrix symbolize the velocity variations with the best correlation between the stretched ACFs and the reference trace. (http://gji.oxfordjournals.org/lookup/suppl/doi:10.1093/gji/ggv529/-/DC1)

Please note: Oxford University Press is not responsible for the content or functionality of any supporting materials supplied by the authors. Any queries (other than missing material) should be directed to the corresponding author for the paper.